Enhancement of magnetic entropy change in La$_{0.57}$Nd$_{0.1}$Sr$_{0.33-x}$Ca$_{x}$MnO$_3$ manganites

Gönül Akça[1,*]

[1] Department of Physics, Faculty of Science and Letters, Çukurova University, Adana 01330, Turkey

ABSTRACT

In present work, structural, magnetic, and magnetocaloric properties of La$_{0.57}$Nd$_{0.1}$Sr$_{0.33-x}$Ca$_{x}$MnO$_3$ (0.0 ≤ x ≤ 0.3) samples have been studied. The conventional solid-state method was used to prepare the samples. The structural properties of the samples were investigated by X-ray diffractometer and scanning electron microscopy. All samples crystallized in rhombohedral structure. The samples consist of grains of different polygonal shape and size. The temperature dependence of magnetization measurements was performed to determine magnetic phase transition temperature. It is observed that the magnetic phase transition temperature decreases with increasing Ca concentration. Magnetic entropy change ($-\Delta S_M$) values of the samples were calculated from the magnetic field dependence of the magnetization based on Maxwell's relation. An enhancement in the $-\Delta S_M$ value was observed with increasing Ca concentration. The maximum magnetic entropy change ($-\Delta S_M^{max}$) value was calculated as 5.85 Jkg^{-1} K^{-1} under 2 T magnetic fields for La$_{0.57}$Nd$_{0.1}$Sr$_{0.03}$Ca$_{0.30}$MnO$_3$ sample. The increase in Ca concentration also caused an increase in the relative cooling power value (RCP). The nature of the magnetic phase transition for the samples was determined using the Banerjee criteria and Franco's universal master curve. The magnetic phase transition type is found as second order for all samples.

1 Introduction

Energy consumption is increasing rapidly day by day due to the increasing human population and industrial growth. The required energy is provided from non-renewable and limited fossil fuels. In addition to these, fossil fuels directly cause an increase in CO$_2$ emissions [1]. For the future of our world, it is imperative to make regulations in areas with high energy consumption in order to save energy and reduce its negative effects on the environment. Priority arrangements should be made in cooling technologies that consume too much energy and cause climate change and global warming [2]. Today, cooling technologies based on the gas compression principle are widely used. These systems have negative effects on the environment, and their energy consumption is quite large [3]. In addition, since the

arrangements that can be made to increase the energy efficiency of these systems are limited and require high costs, it is necessary to work on the development of new systems that could be used instead of these systems.

Magnetic refrigeration (MR) systems with better energy consumption and efficiency [4] are considered the future cooling system. It is known that MR systems are also eco-friendly since a solid magnetic material is used as a cooling element in these systems [5]. The working principle of MR systems is magnetocaloric effect (MCE), which is defined as the change in the temperature of the magnetic material as a result of the change in the entropy of a magnetic material subjected to a magnetic field [6, 7]. The magnetocaloric properties of a material are defined by two fundamental quantities: magnetic entropy change ($-\Delta S_M$) and adiabatic temperature change (ΔT_{ad}) [8]. The ΔT_{ad} value is determined using direct methods, while $-\Delta S_M$ is calculated indirectly from magnetization measurements depending on magnetic field [9].

Gadolinium (Gd) and Gd alloys have been used as cooling elements in many MR systems designed and developed to date [10, 11]. However, commercial use of these MR systems is not possible for some reasons [8, 11–13]. In the view of the applications, the most essential requirement is to provide new materials with large MCE in a low magnetic field and near room temperature. In addition, the type of magnetic phase transition and relative cooling power (RCP) are critical parameters [8].

Perovskites, which exhibit extraordinary chemical and physical properties, are one of the most intensively researched samples and have influential applications in many fields [14–16]. Magnetocaloric properties of La-based perovskite manganites have been studied in detail due to various properties such as high chemical stability, adjustable magnetic phase transition temperature, inexpensive raw material, and $-\Delta S_M$ comparable to Gd [17–21]. The ratio between the number of Mn^{4+} and Mn^{3+} ions (depends on the doping level, x), the average size of the cation at the A-site ($\langle r_A \rangle$) [22], and the degree of disorder at the A-site [23] affect the magnetic and magnetocaloric properties of manganites. Among the studied La-based manganites, $La_{0.57}Nd_{0.1}Sr_{0.33}MnO_3$ sample shows paramagnetic (PM)-ferromagnetic (FM) phase transition above room temperature [24]. Ca-doped La-based manganites exhibit magnetic

phase transition below room temperature and have acceptable $-\Delta S_M$[25]. In the literature, there are studies reporting $-\Delta S_M$ values of Ca-doped $LaMnO_3$ manganites are comparable to Gd, and Ca content induces an increment in $-\Delta S_M$ values [26–28]. Ca ion has 2 + valence state and its ionic radius is smaller than Sr but close to La and Nd ions [29]. In the case of partial Ca addition, the Mn^{3+}/ Mn^{4+} ratio remains constant, while a change occurs in the $\langle r_A \rangle$ and the degree of disorder at the A site. This plays a critical role in the variation of magnetic and magnetocaloric properties. Moreover, it is possible to say that T_C increases with increasing Sr concentration, and $-\Delta S_M$ value affects positively with increment in Ca-content [30–32]. In this study, the structural, magnetic, and magnetocaloric properties of $La_{0.57}Nd_{0.1}Sr_{0.33-x}Ca_xMnO_3$ ($0.0 \leq x \leq 0.3$) manganites have been investigated in detail. The main aim of this study is to adjust the T_C towards room temperature by partial substitution of Sr with Ca in the $La_{0.57}Nd_{0.1}Sr_{0.33}MnO_3$ manganite system.

2 Experimental details

In this study, $La_{0.57}Nd_{0.1}Sr_{0.33-x}Ca_xMnO_3$ (x = 0.0, 0.10, 0.20, and 0.30) manganite samples were prepared by solid-state method. La_2O_3 (99.99%, Sigma Aldrich), Nd_2O_3 (99.99%, Sigma Aldrich), SrO (99.99%, Sigma Aldrich), CaO (99.995%, Sigma Aldrich), and MnO_2 (99.99%, Sigma Aldrich) starting materials were used. The starting compounds were weighed in accordance with stoichiometric ratios. By using an agate mortar, the weighed raw materials were mixed and ground for a total 60 min (6 times 10 min). Afterwards, the mixture was calcined at 600 °C for 6 h. The grinding and mixing processes were repeated under the same conditions. Finally, the samples were pelleted and sintered at 1200 °C for 24 h. In forthcoming sections, the final samples were labeled as LNSM, LNSCM-1, LNSCM-2, and LNSCM-3 for undoped and 1%, 2%, and 3% Ca-added samples, respectively. To obtain information about crystal symmetry, lattice parameters and unit cell volume of the samples, X-ray diffraction (XRD) measurements were performed by a Philips PANalytical Empyrean X-ray diffraction meter. The XRD data were collected at room temperature in 0.0131 degree increments over the range of 20–80°. Scanning electron microscope (SEM) with energy dispersive X-

ray spectrometry (EDS) was used to investigate the grain structure and elemental analysis of the samples. Magnetic measurements depending on temperature ($M(T)$) and magnetic field ($M(H)$) were performed by a physical property measurement system (PPMS) equipped with a vibrating sample magnetometer (VSM) module. In order to determine the magnetic phase transition temperature, described as Curie temperature (T_C), a 10 mT weak field was applied to the samples in zero–field-cooled (ZFC) and field-cooled (FC) modes in the temperature range of 5–380 K. The magnetization measurements as a function of the magnetic field were made to calculate the $-\Delta S_M$ of the samples and to identify the type of magnetic phase transition.

3 Results and discussion

The XRD patterns of the samples recorded at room temperature are given in Fig. 1. The observed and calculated diffraction patterns were represented by solid circles and lines, respectively. Bragg positions are marked with green vertical bars. The difference between the observed and calculated diffraction pattern was shown by the blue line. In the experimental test range, it was determined that the samples consisted of a single phase. The structural parameters of the samples were refined using Rietveld's profile-fitting method [33] and results are given in Table 1. The lattice parameters of the samples do not show a systematic change with the increasing Ca concentration. However, the unit cell volume of the samples decreases almost linearly with the increasing Ca concentration. It is thought that this decrement may be related to the smaller ionic radius of the Ca^{2+} ion than Sr^{2+} ion [29]. The samples were crystallized in rhombohedral structure. Goldschmidt tolerance factor (t_G) which is defined as the geometric measure of the size mismatch of perovskite, is given by the following formula [32]:

$$t_G = \frac{(\langle r_A \rangle + r_O)}{\sqrt{2}(\langle r_B \rangle + r_O)}. \tag{1}$$

In the equation, the average ionic radii of A and B-site are denoted by $\langle r_A \rangle$ and $\langle r_B \rangle$, respectively. The ionic radius of the oxygen ion is abbreviated as r_O. It is known that the perovskite structure is preserved within the limits of $0.75 < t_G < 1.0$ [32]. The crystal structure is cubic, rhombohedral, and orthorhombic

for $t_G = 1$, $0.96 < t_G < 1.0$, and $t_G < 0.96$, respectively [34]. Based on Shannon's list of effective ionic radii, $\langle r_A \rangle$ and t_G values of the samples were calculated for coordination number 12. According to t_G value given in Table 1, it was confirmed that the samples were crystallized in rhombohedral symmetry. It was observed that the crystal symmetry of the samples did not change, although increasing Ca concentration caused a decrease in $\langle r_A \rangle$ and t_G values. The physical properties of the manganites also change with A-site disorder induced by the A-site ionic radius variance, (σ^2), given in the following equation [35, 36]:

$$\sigma^2 = \sum (q_i r_i^2 - \langle r_A \rangle^2, \tag{2}$$

where q_i and r_i show atomic concentration and ionic radius of the i-type ion, respectively. Calculated σ^2 values for samples decrease linearly with increasing Ca concentration. It is inevitable that this result will cause a change in the magnetic and magnetocaloric properties of the samples.

Using the Scherrer formula, the average crystallite size (D_{XRD}) can be calculated from the following equation [37]:

$$D_{XRD} = \frac{\kappa \lambda}{\beta \cos \theta}, \tag{3}$$

where λ and κ are the X-ray wavelength (Cu–K$_\alpha$ = 1.5406 Å) and crystallite shape factor (0.9), respectively. β is the peak full width at half maximum at the observed peak angle. D_{XRD} values calculated from the most intense XRD peaks of the samples are given in Table 1. For LNSM sample, this value was calculated as 67.4 nm. Although this value initially increased with the replacement of Sr with Ca, a linear decrease observed with the increase of Ca ratio.

The chemical compositions of the samples were examined by EDS analysis. Figure 2 shows the EDS spectra of the samples. All samples contain the expected chemical elements and no trace of impurity elements. The atomic percentages of the samples are given in Table 2. The obtained compositions from EDS are very close to the nominal compositions of the samples. The SEM images of the samples are given insets of Figs. 2. It can be seen that the samples consist of different polygonal-shaped grains with different sizes, and the boundaries of the grains are clear. There is no linear variation between Ca concentration and grain size. However, it was observed that the clarity of the grains boundaries increased with the increase in Ca concentration.
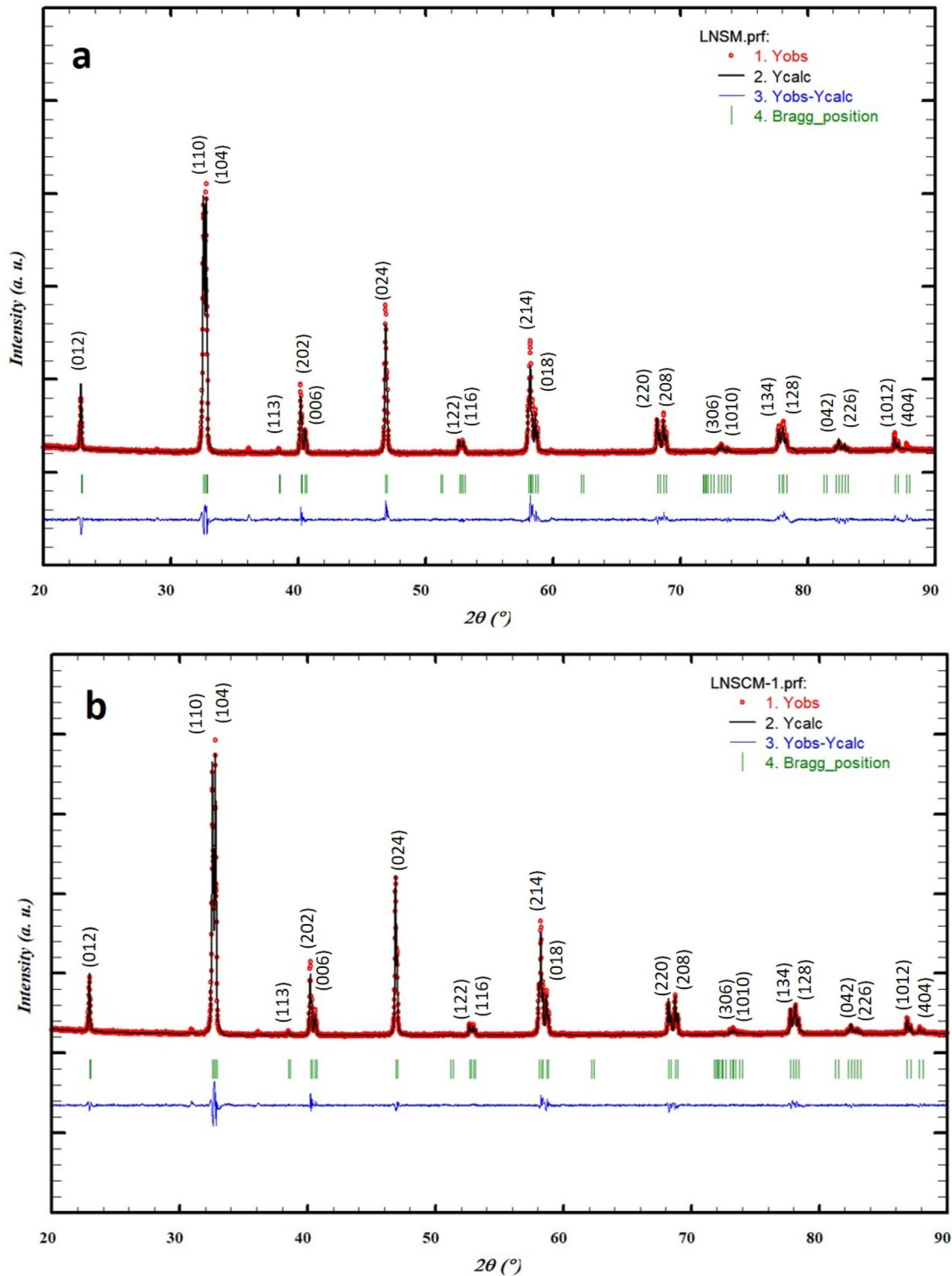
Fig. 1 XRD patterns of $La_{0.57}Nd_{0.1}Sr_{0.33-x}Ca_xMnO_3$ $(0.0 \leq x \leq 0.3)$ samples **a** LNSM, **b** LNSCM-1, **c** LNSCM-2, **d** LNSCM-3

Figure 3 shows the $M(T)$ curves obtained under a weak magnetic field of 10 mT at ZFC (open circle) and FC (solid circle) modes in the temperature range of 5–380 K. While the ZFC and FC curves diverge from each other by following an irreversible path in the FM region, they show a reversible trend in the PM
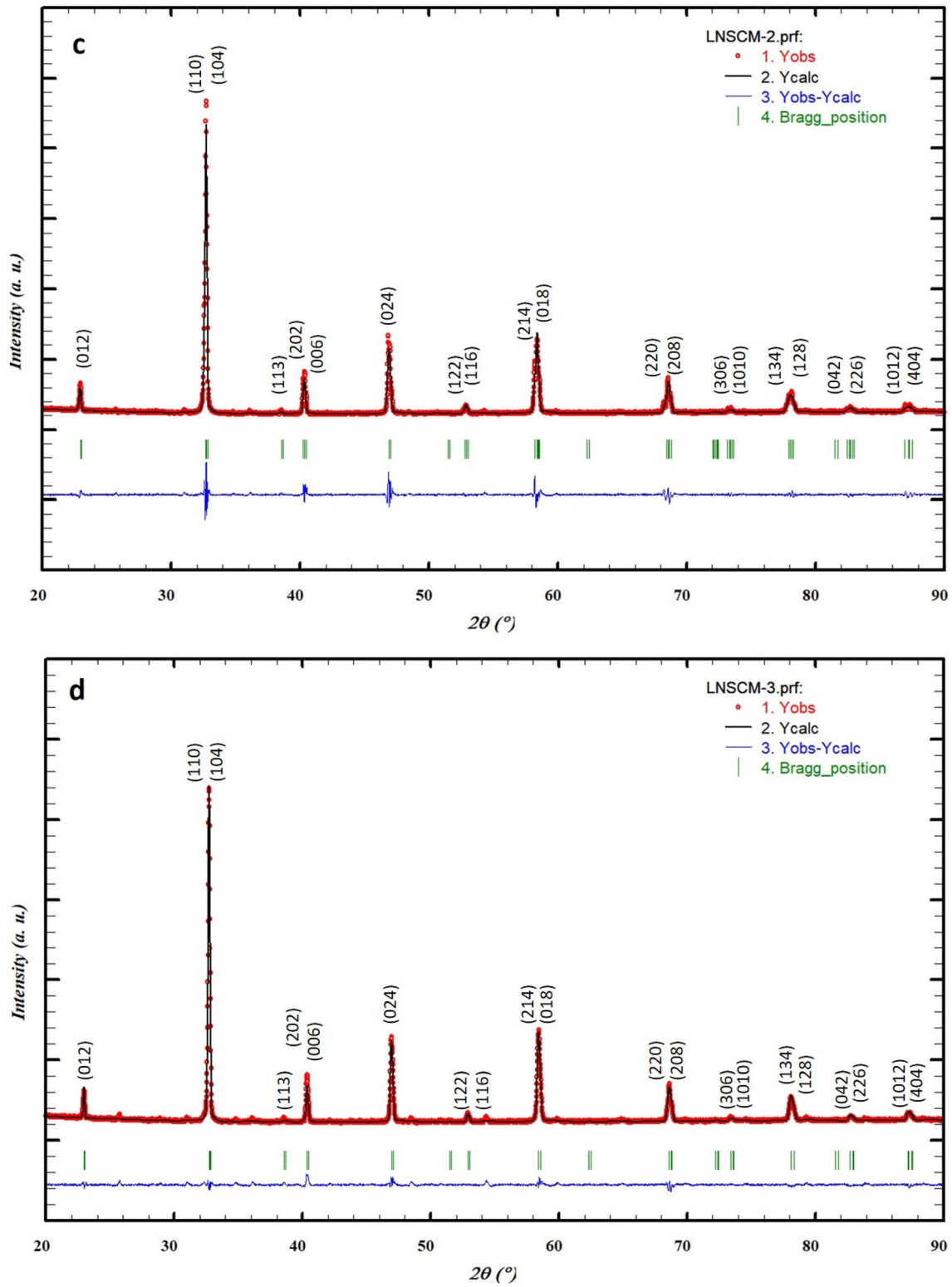
Fig. 1 continued

Table 1 Structural parameters of the $La_{0.57}Nd_{0.1}Sr_{0.33-x}Ca_xMnO_3$ ($0.0 \leq x \leq 0.3$) samples

Samples	LNSM	LNSCM-1	LNSCM-2	LNSCM-3
$a = b$(Å)	5.4961	5.4944	5.4671	5.4673
c (Å)	13.3367	13.3249	13.4364	13.3951
V (Å^3)	348.8963	348.3674	347.7940	346.8561
$< r_A >$ (Å)	1.3774	1.3674	1.3574	1.3474
t_G	0.9785	0.9749	0.9714	0.9679
σ^2 (Å^2)	0.0026	0.0023	0.0017	0.0010
Rp	17.9	13.1	16.4	16.2
Rwp	14	10.6	10.7	12.6
$Rexp$	5	4.58	6.02	6.28
$\chi 2$	3.95	3.62	3.99	3.94
D_{XRD}(nm)	67.4	84.8	57.7	55.6

region. This bifurcation can occur for a variety of reasons, such as magnetic inhomogeneity [38], domain pinning effect [39], and canted nature of the spins [18]. In the PM-FM transition region, ZFC and FC curves exhibit a sharp transition. It promisingly implies a high $-\Delta S_M$ [39, 40]. An increase was observed in the ZFC and FC curves of the LNSCM-1 sample (see Fig. 3b), indicating the presence of a charge-ordering (CO) state [41]. The T_C is mostly determined from the inflection point of dM/dT curve obtained from the $M(T)$ curve. Figure 4a represents the dM/dT curves of the samples. These curves have a single inflection peak. This implies that samples contain a single magnetic phase. T_C decreased from 356 to 224 K with increasing Ca concentration (from x = 0.0 to 0.30). When Ca^{2+} is substituted for Sr^{2+} in the samples, the Mn^{3+}/Mn^{4+} ratio does not change. However, the $\langle r_A \rangle$ and σ^2 values of the samples decrease with increasing Ca concentration due to the difference between the ionic radii of Ca and Sr ions. As a result, the structural distortions occur, and a decrement in T_C value can be observed. This may arise from the decreasing of $\langle r_A \rangle$ and σ^2 values [31]. The obtained results are compatible with those reported in the literature [42, 43]. Figure 4b shows the temperature dependence of the inverse magnetic susceptibility, $1/\chi(T)$, of the curves obtained using the ZFC magnetization data. The $1/\chi(T)$ and the fitting results by using the Curie Weiss (CW) law are presented by symbols and lines, respectively. In the paramagnetic region, for LNSM and LNSCM-1 samples, the $1/\chi(T)$ curve shows a linear variation indicating that it obeys the CW law given by $\chi = C/$

$(T-\theta)$, where C is the Curie constant and θ is the paramagnetic Curie temperature. On the other hand, $1/\chi(T)$ curve of LNSCM-2 and LNSCM-3 samples show a deviation from the CW law pointing out the presence of the Griffiths phase [44]. The θ value of the samples was determined from the $1/\chi(T)$ curves. The θ values of the samples are given in Table 2. The positive value of θ implies that the interaction between the nearest spins is the FM [45]. It is seen that the θ value is slightly larger than the T_C value for LNSCM-2 and LNSCM-3 samples. This difference may be due to the presence of short-range FM order related to the existence of magnetic inhomogeneity above T_C [46]. The θ temperature shows a reduction with increasing Ca concentration. This verifies the weakening FM double exchange interactions [47]. The C constant is given by $C = \frac{N_A \mu_B^2}{3k_B} \mu_{eff}^2$; where $N_A,$ $k_B,$ and μ_B represent Avogadro's number, Boltzman's constant, and the Bohr magneton, respectively. The μ_{eff} denotes effective magnetic moment. To calculate the experimental $\mu_{eff}\left(\mu_{eff}^{exp}\right)$, C constant is derived from the linear fitting of $1/\chi(T)$ curve of the samples. By using C constant equation, the μ_{eff}^{exp} value was calculated experimentally as 2.89, 2.44, 2.40, and $2.61\mu_B$ for LNSM, LNSCM-1, LNSCM-2, and LNSMC-3 samples, respectively. The μ_{eff}^{exp} values show a nonlinear variation with increasing Ca concentration. This may be related to the order of magnetic inhomogeneity of the samples. The theoretical effective magnetic moment $\left(\mu_{eff}^{theo}\right)$ was calculated by using the following equation [48]:

$$\mu_{eff}^{theo} = \sqrt{0.67\left[\mu_{eff}\left(Mn^{3+}\right)\right]^2 + 0.33\left[\mu_{eff}\left(Mn^{4+}\right)\right]^2 + 0.1\left[\mu_{eff}\left(Nd^{3+}\right)\right]^2}$$

(4)

where $\mu_{eff}\left(Mn^{3+}\right) = 4.9$, $\mu_{eff}\left(Mn^{4+}\right) = 3.87$, and $\mu_{eff}\left(Nd^{3+}\right) = 3.62 \ \mu_B$ [49]. The μ_{eff}^{theo} value is larger than the μ_{eff}^{exp} value derived from the linear fitting of $1/\chi(T)$ curve. According to the results, it can say that large spin ordering occurs in samples. Similar results have been observed in manganites [46, 50].

To obtain deep information about the magnetic behavior of the samples, the $M(H)$ measurements have been performed up to 5 T with a temperature increase of 4 K around T_C. Figure 5 shows the $M(H)$ curves of the samples. Below T_C, the magnetization of the samples varies rapidly with the applied magnetic
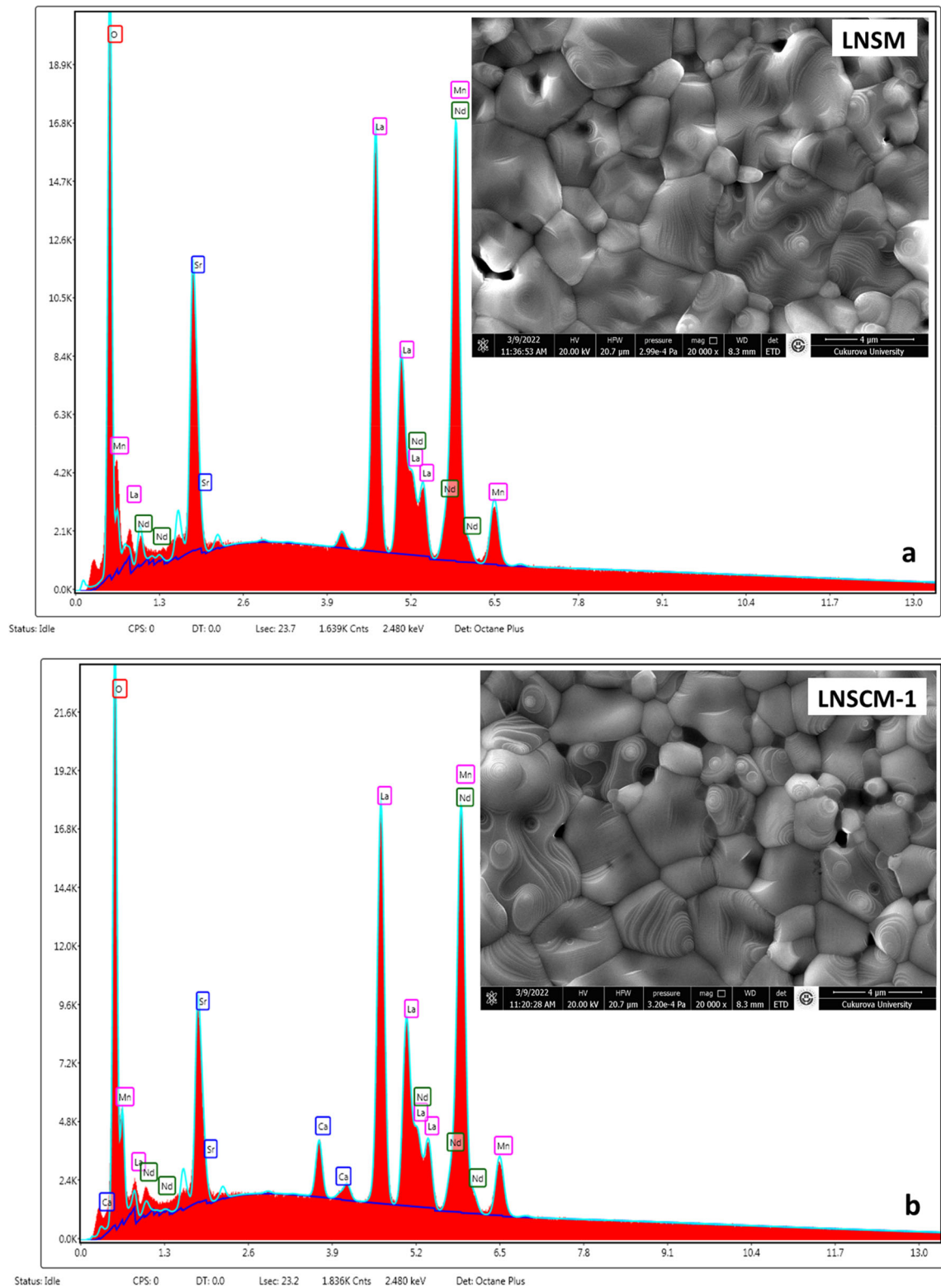
Fig. 2 EDS graphs of $La_{0.57}Nd_{0.1}Sr_{0.33-x}Ca_xMnO_3$ ($0.0 \leq x \leq 0.3$) samples **a** LNSM, **b** LNSCM-1, **c** LNSCM-2, **d** LNSCM-3. Insets show SEM images of the samples at 20 KX magnification
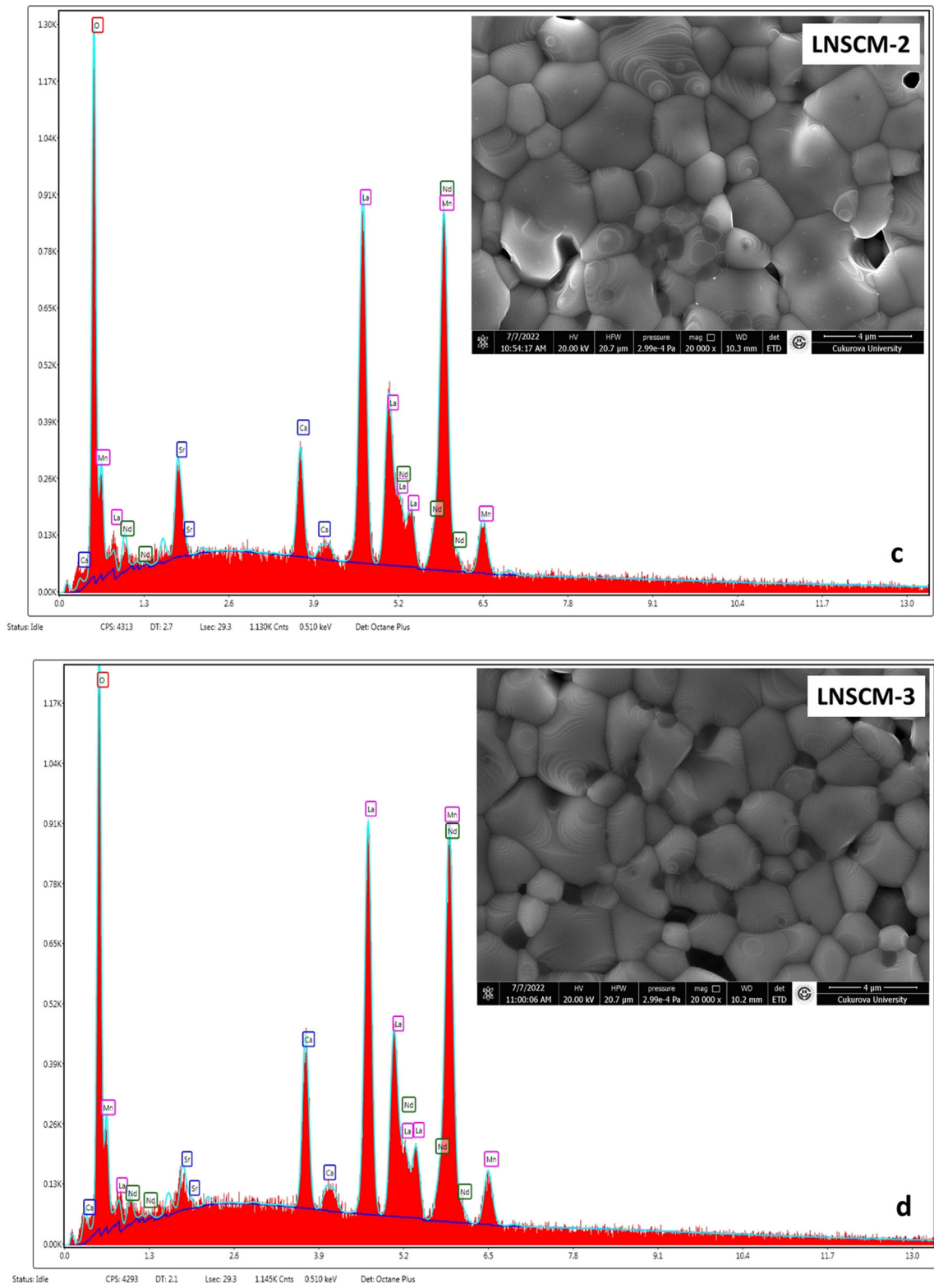
Fig. 2 continued

Table 2 Atomic percentages of the $La_{0.57}Nd_{0.1}Sr_{0.33-x}Ca_xMnO_3$ $(0.0 \leq x \leq 0.3)$ samples

Samples	Atomic percentages (%)					
	La	Nd	Sr	Ca	Mn	O
LNSM	12.48	2.38	6.02	-	22.34	56.78
LNSCM-1	12.23	2.3	4.44	1.86	21.36	57.81
LNSCM-2	12.57	2.31	2.41	3.8	21.26	57.65
LNSCM-3	12.29	2.1	1.1	5.54	21.48	57.49

field and reaches saturation above 0.5 T. This behavior is characteristic property of FM material. Except for the LNSM sample, the $M(H)$ curves show a linear variation with the magnetic field at temperatures above T_C. The linear variation of the $M(H)$

curves of the materials with the applied field confirms that the samples exhibit PM properties at temperatures above T_C. As seen in Fig. 5a, the $M(H)$ curve of the LNSM sample does not exhibit a linear variation, indicating that it does not show pure paramagnetic properties, which may arise from the presence of FM clusters on the T_C [51, 52]. Above and below T_C, the behavior of the $M(H)$ curves confirms a magnetic phase transition from FM to PM with increasing temperature. The results obtained from $M(H)$ measurements are in agreement with $M(T)$. The $M(H)$ curves of the LNSCM-3 sample (see Fig. 5d) show a S-shaped change in the temperature region of 212–252 K. This change points to the metamagnetic transition, which expresses the coexistence of FM and AFM (antiferromagnetic)-CO phases [53]. The
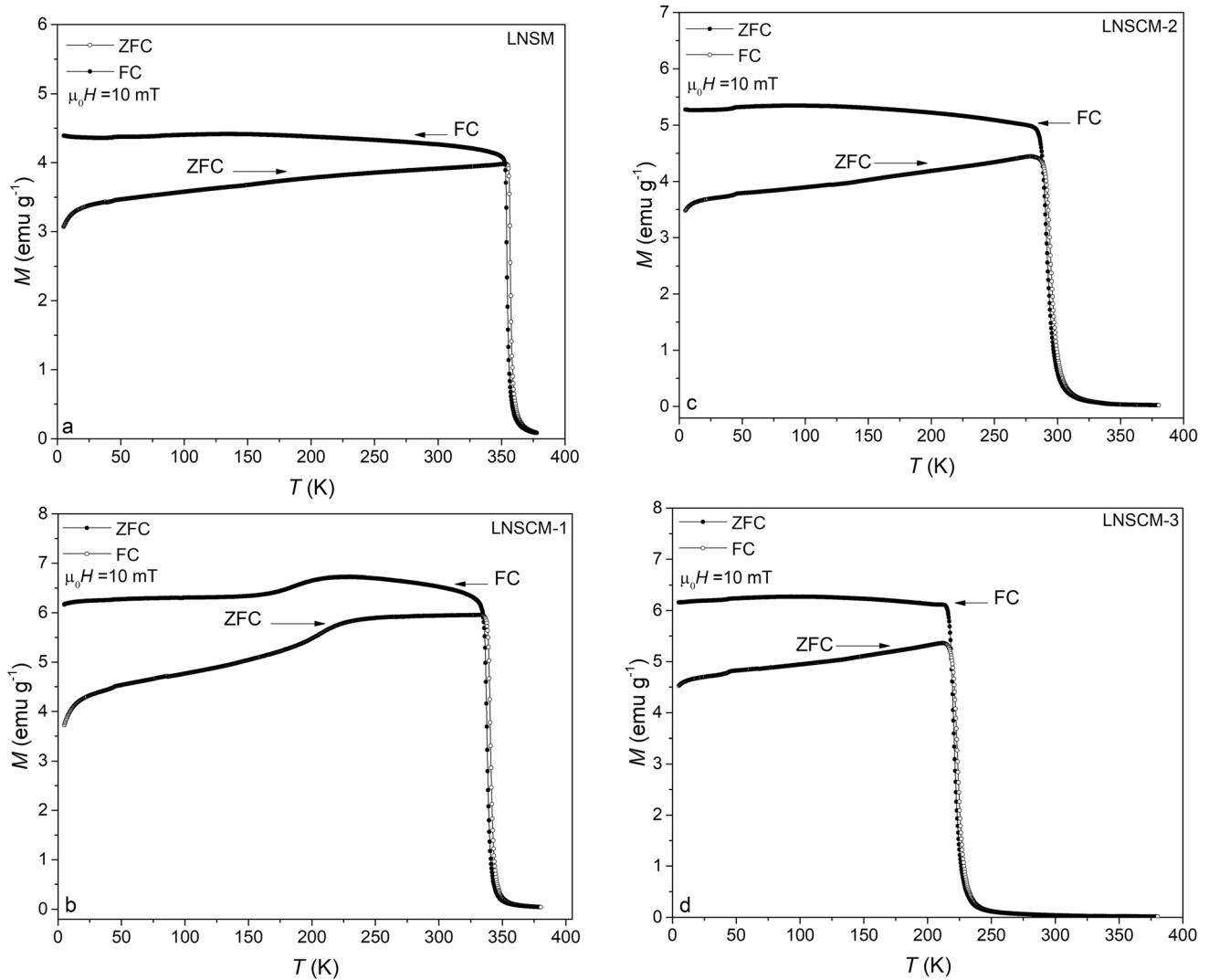

Fig. 3 The $M(T)$ curves of $La_{0.57}Nd_{0.1}Sr_{0.33-x}Ca_xMnO_3$ $(0.0 \leq x \leq 0.3)$ samples **a** LNSM, **b** LNSCM-1, **c** LNSCM-2, **d** LNSCM-3

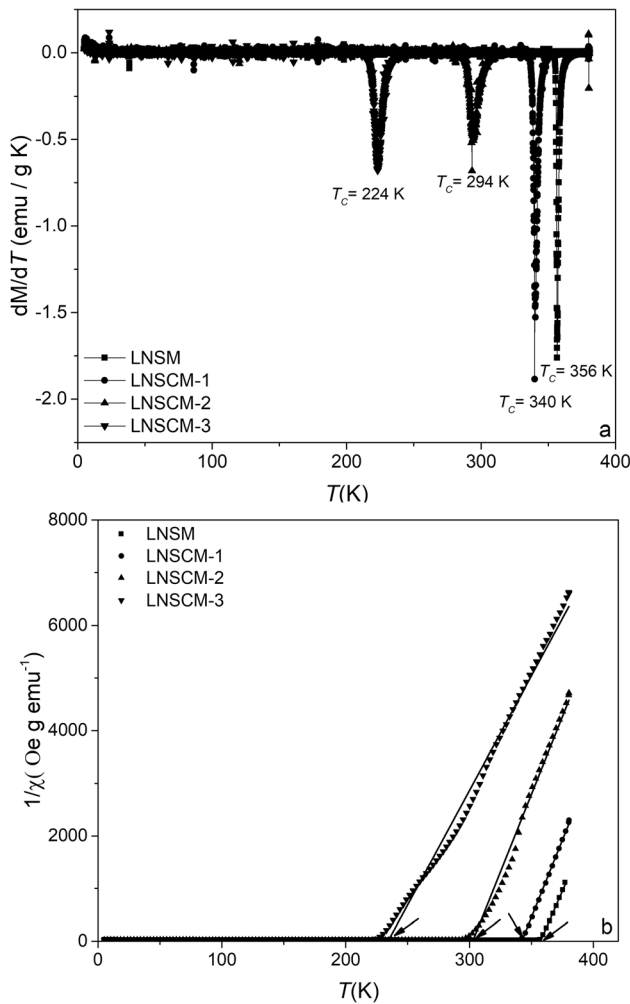**Fig. 4** **a** dM/dT (T) and **b** $1/\chi(T)$ curves of La$_{0.57}$Nd$_{0.1}$Sr$_{0.33-x}$Ca$_x$MnO$_3$ ($0.0 \leq x \leq 0.3$) samples

metamagnetic transition indicates the possibility of a large $-\Delta S_M$ around T_C [54].

The numerical value of $-\Delta S_M$ is calculated by using the following equation [55];

$$-\Delta S_M(H,T) = \sum \frac{M_i - M_{i+1}}{T_{i+1} - T_i} \Delta H_i \qquad (5)$$

where the experimental values of magnetization under the magnetic field H_i at temperatures T_i and T_{i+1} are represented by M_i and M_{i+1}, respectively. The $-\Delta S_M$ values of the samples were calculated for different magnetic fields, and the temperature dependence of the $-\Delta S_M$ values ($-\Delta S_M$ (T)) was obtained. Figure 6 shows the $-\Delta S_M$ (T) curves of the samples. Around T_C, the $-\Delta S_M$ (T) curves exhibit a maximum peak called as maximum magnetic entropy change value ($-\Delta S_M^{max}$). The value of $-\Delta S_M^{max}$ increases with increasing applied magnetic field. This

is related to the orientation of the magnetic moments with the magnetic field [56]. The $-\Delta S_M^{max}$ value of the samples for 2 T was calculated as 2.53, 2.85, 3.17, and 5.85 Jkg^{-1} K^{-1} for LNSM, LNSCM-1, LNSCM-2, and LNSCM-3, respectively. It is observed that the $-\Delta S_M^{max}$ values of the samples enhance with increasing Ca concentration in agreement with the literature [30, 57]. A comparison of the $-\Delta S_M^{max}$ values of LNSCM-2 and LNSCM-3 samples with similar materials reported in the literature has given in Table 4 [24, 49, 58–62]. The $-\Delta S_M^{max}$ value of the LNSCM-3 sample is larger than that obtained in Gd [63]. However, this sample shows a magnetic phase transition at 224 K. Therefore, this sample can be considered as a cooling sample for low-temperature MR applications. Moreover, the LNSCM-2 sample, which transitions around room temperature, may be a good candidate for room temperature MR applications as it has an acceptable value of $-\Delta S_M^{max}$ under low magnetic field.

One of the critical criteria in consideration of a material as a cooling element for magnetic cooling systems is RCP. This parameter can be calculated from $-\Delta S_M$ (T) curves by RCP = $\left| -\Delta S_M^{max} \right| \times \delta T_{FWHM}$ where δT_{FWHM} is the full width at half maximum of the $-\Delta S_M$ (T). The RCP value for 2 T of the samples was determined and is given in Table 3. The RCP value of the samples shows a linear increment with increasing Ca concentration. The RCP value of other magnetic compounds is listed in Table 4 for comparison purposes.

Magnetocaloric materials are classified as first- and second-order magnetic phase transition in terms of the nature of magnetic phase transition. Since first-order magnetocaloric materials show thermal and magnetic hysteresis, they are not favorable for magnetic cooling systems. Although both groups have advantages and disadvantages relative to each other, the material that can be used for magnetic cooling systems should exhibit a second-order phase transition since it does not show thermal and magnetic hysteresis [64]. The character of magnetic phase transition is generally used by the Banerjee criterion [65]. According to this criterion, Arrott curves (H/M vs. M^2) are obtained by using the data obtained from the $M(H)$ measurements. The sign of the slope of these curves plays a decisive role in determining the type of magnetic phase transition. Around T_C, the positive slope of Arrott plots indicates the second-
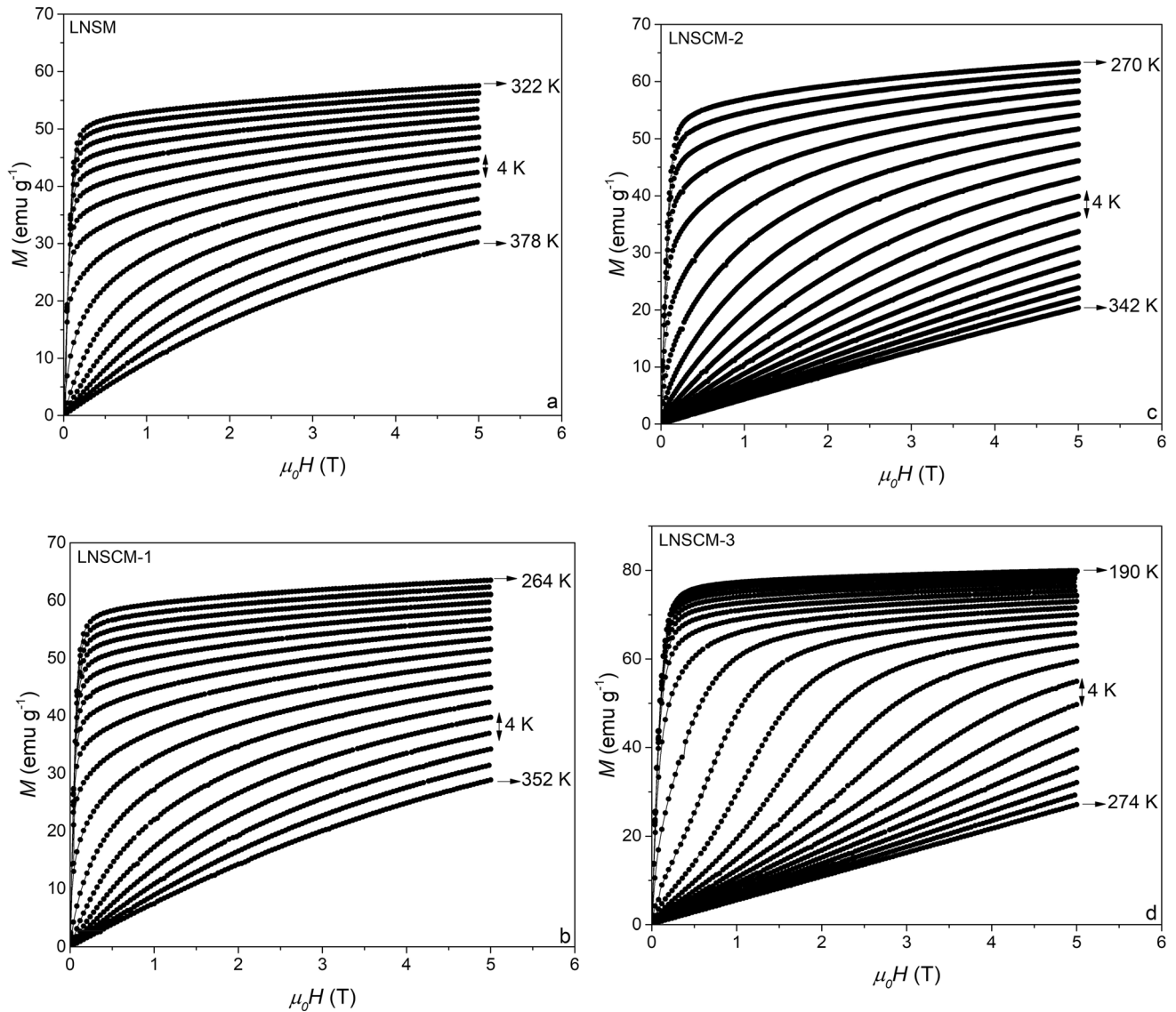
Fig. 5 The $M(H)$ curves of La$_{0.57}$Nd$_{0.1}$Sr$_{0.33-x}$Ca$_x$MnO$_3$ ($0.0 \leq x \leq 0.3$) samples **a** LNSM, **b** LNSCM-1, **c** LNSCM-2, **d** LNSCM-3

order magnetic phase transition, while the negative slope indicates first-order magnetic phase transition. Figure 7 shows the Arrott plots of the samples. It is possible to say that these samples exhibit a second-order magnetic phase transition due to the positive slope of the Arrott plots around T_C. Another method for determining magnetic phase transition characteristic is universal master curve proposed by Franco et al. [66]. According to this method, the universal curve can be normalized to each isofield $-\Delta S_M(T)$ curves by using $-\Delta S_M^{max}$ and rescaling the temperature axis based on the following equations:

$$\theta = \begin{cases} -(T - T_C)/(T_{r1} - T_C) & T \leq T_C \\ (T - T_C)/(T_{r2} - T_C) & T > T_C \end{cases} \tag{6}$$

In Eq. 6, T_{r1} and T_{r2} represent the temperatures above and below T_C. The universal curve of the samples is given in Fig. 8. It is observed that the curves obtained from different magnetic fields overlap. This indicates that a second-order magnetic phase transition has occurred [67]. Hence, it can be said that Banerjee criterion and Franco's universal curve method are in good agreement with each other for the samples studied.

Amaral et al. [68–70] have proposed a succeeding model based on Landau's theory to explain the
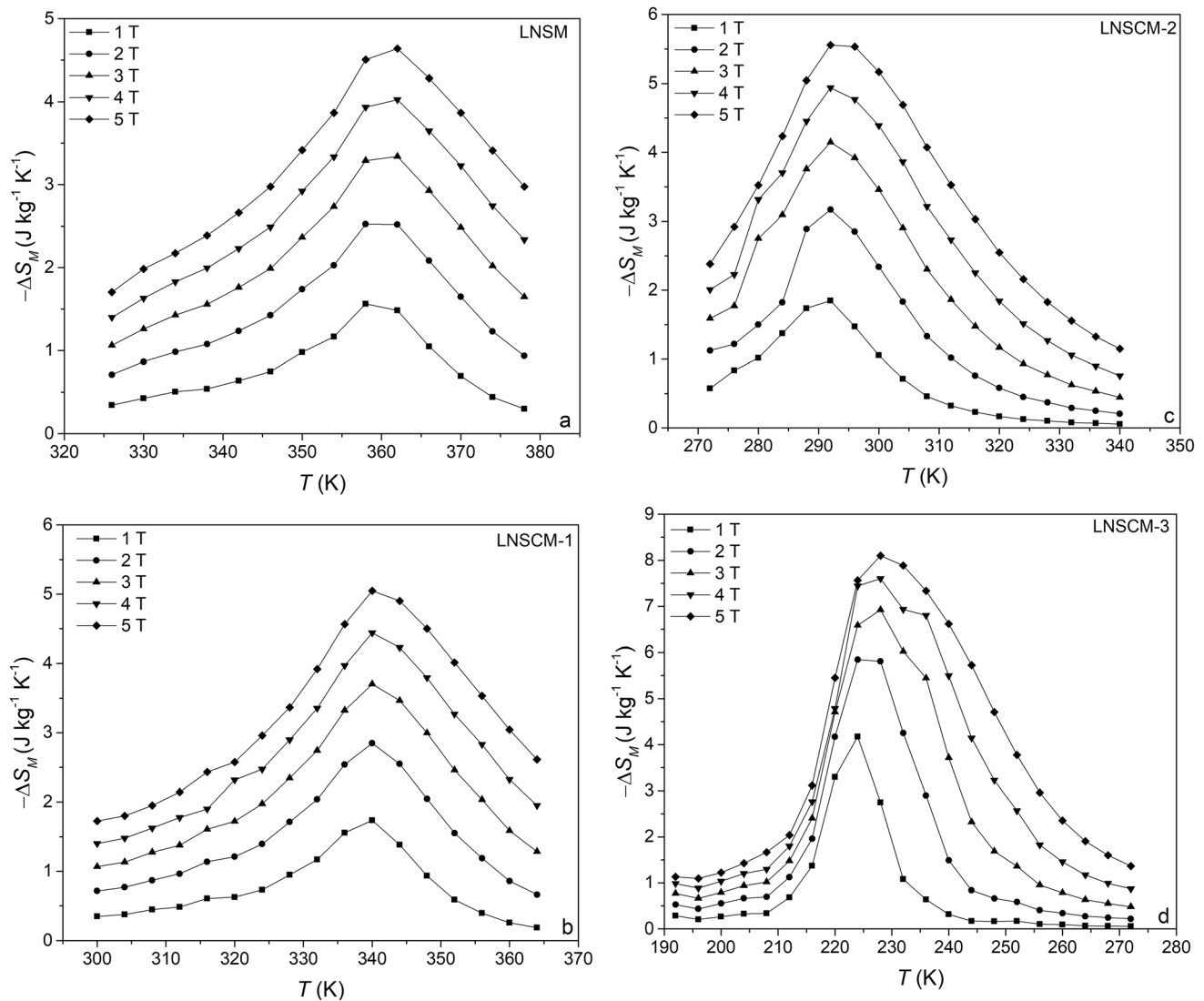
Fig. 6 $-\Delta S_M(T)$ curves of $La_{0.57}Nd_{0.1}Sr_{0.33-x}Ca_xMnO_3$ ($0.0 \leq x \leq 0.3$) samples **a** LNSM, **b** LNSCM-1, **c** LNSCM-2, **d** LNSCM-3

Table 3 The temperatures T_C and θ and some magnetocaloric properties of the $La_{0.57}Nd_{0.1}Sr_{0.33-x}Ca_xMnO_3$ ($0.0 \leq x \leq 0.3$) samples

Samples	T_C (K)	θ (K)	ΔH (T)	$-\Delta S_M^{max}$ (Jkg^{-1} K^{-1})	δT_{FWHM} (K)	RCP (Jkg^{-1})
LNSM	356	357	2	2.53	31.02	78.48
LNSCM-1	340	343	2	2.85	29.34	83.62
LNSCM-2	294	303	2	3.17	28.22	89.46
LNSCM-3	224	230	2	5.85	17.87	104.54

contribution of magnetoelastic and electron interactions in manganites. From energy minimization, a magnetic equation of state based on this theory can be written as follows [69]:

$$\frac{H}{M} = A + BM^2 + CM^4. \tag{7}$$

Magnetic entropy is obtained by differentiating the magnetic part of the free energy with respect to the temperature.

$$S_M(T,H) = -\frac{1}{2}A'(T)M^2 - \frac{1}{4}B'(T)M^4 - \frac{1}{6}C'(T)M^6 \tag{8}$$

Table 4 Comparison of $-\Delta S_M^{max}$ and RCP values of LNSCM-2 and LNSCM-3 samples with some similar manganites found in the literature

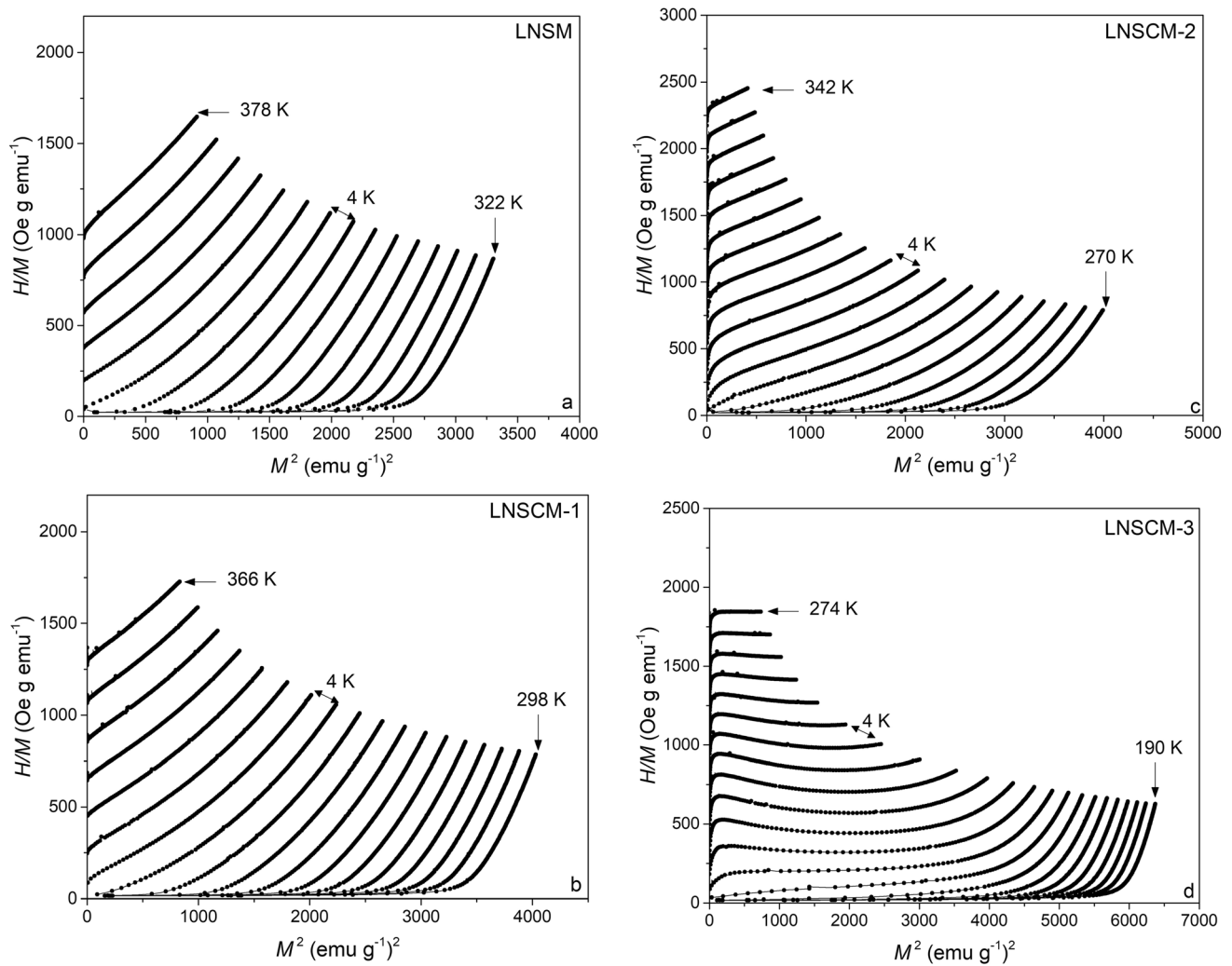| Samples	ΔH (T)	$-\Delta S_M^{max}$ (Jkg^{-1} K^{-1})	RCP (Jkg^{-1})	Ref
LNSCM-2	2	3.17	89.46	This work
LNSCM-3	2	5.85	104.54	This work
La$_{0.57}$Nd$_{0.1}$Sr$_{0.33}$MnO$_3$	1	2.31	23	[24]
La$_{0.7}$Sr$_{0.2}$Nd$_{0.1}$Mn$_{0.95}$Ni$_{0.0}$5O$_3$	2	2.96	156.23	[49]
(La$_{0.9}$Pr$_{0.1}$)$_{0.85}$Ag$_{0.15}$MnO$_3$	2	4.73	80.24	[58]
La$_{0.57}$Nd$_{0.1}$Sr$_{0.18}$MnO$_3$	5	4.36	214	[59]
La$_{0.57}$Nd$_{0.1}$Sr$_{0.33}$Mn$_{0.90}$Sn$_{0.10}$O$_3$	5	3.22	56	[60]
La$_{0.7}$Nd$_{0.05}$Ba$_{0.25}$MnO$_3$	5	3.9	231.6	[61]
La$_{0.6}$Nd$_{0.1}$Ca$_{0.15}$Sr$_{0.15}$MnO$_3$	5	3.8	173.66	[62]

Fig. 7 Arrott plots of La$_{0.57}$Nd$_{0.1}$Sr$_{0.33-x}$Ca$_x$MnO$_3$ ($0.0 \leq x \leq 0.3$) samples **a** LNSM, **b** LNSCM-1, **c** LNSCM-2, **d** LNSCM-3

$A'(T)$, $B'(T)$, and $C'(T)$ are the derivatives of the Landau parameters (A, B, and C) given in Eq. 7. The temperature dependence of Landau's parameters can be determined from the linear fitting of the Arrott plots. There is an important physical meaning to

these parameters [71]. Namely, parameter $A(T)$ gives information about magnetic susceptibility and gets minimum and positive values at T_C. To determine magnetic phase transition type, $B(T)$ value at T_C is checked. If its value is positive at T_C, the magnetic
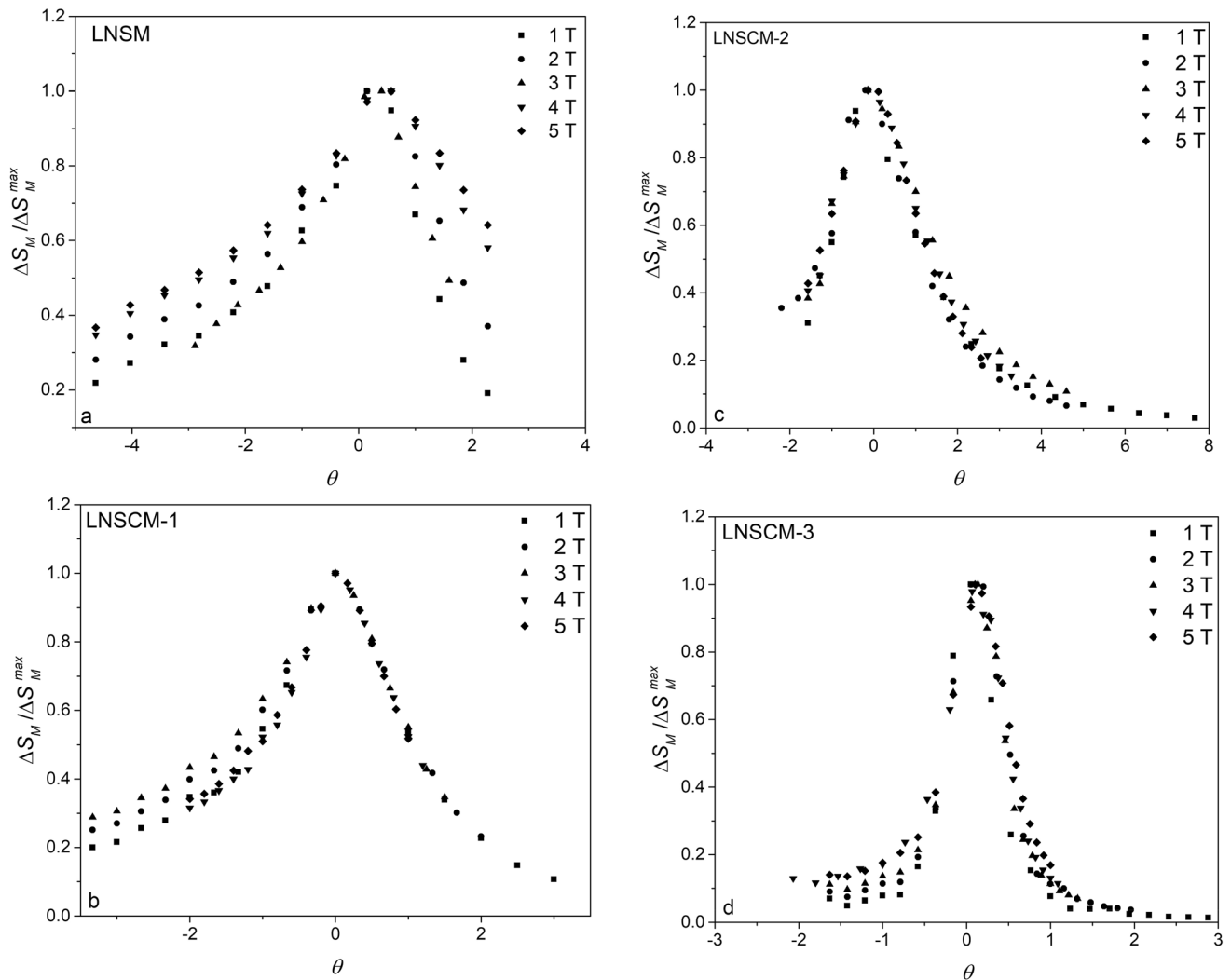
Fig. 8 Rescaled universal master curves obtained under different magnetic fields of La$_{0.57}$Nd$_{0.1}$Sr$_{0.33-x}$Ca$_x$MnO$_3$ (0.0 ≤ x ≤ 0.3) samples **a** LNSM, **b** LNSCM-1, **c** LNSCM-2, **d** LNSCM-3

phase transition is second order; if not, it is first order. The $A (T)$ and $B (T)$ parameters are presented in Fig. 9 (for clarity only LNSCM-2 sample is given). All positive values confirm that the magnetic phase transition is second order for all samples. In addition, the obtained results from Banerjee's criterion, Franco's universal master curve, and Landau's theory are compatible with each other. The $-\Delta S_M$ values of the samples were theoretically calculated for different magnetic fields by using Eq. 8 and the derivatives of Landau's parameters. Figure 10 exhibits the variations of experimental and theoretical values of $-\Delta S_M$ as a function of the temperature under 5 T. Solid symbols and line represent the experimental and theoretical calculation (based on the Landau theory), respectively. The experimental and theoretical $-\Delta S_M$
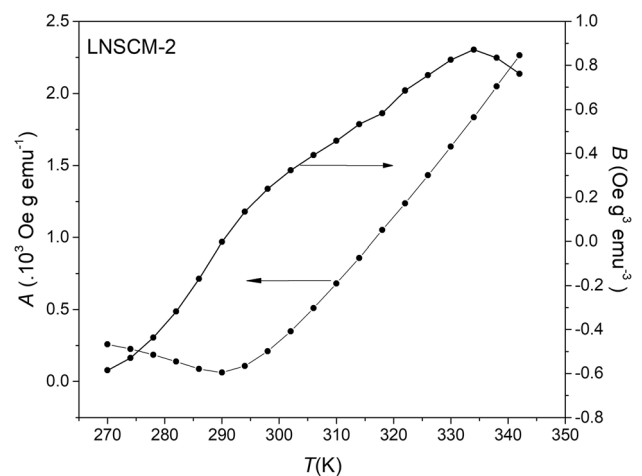

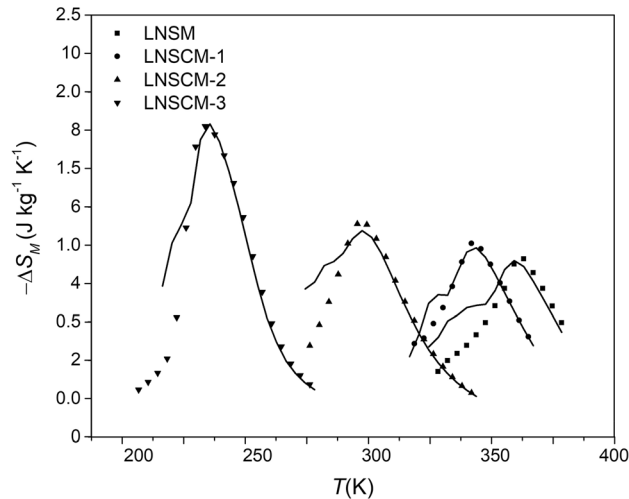**Fig. 9** The temperature dependence of A and B Landau's parameters for LNSCM-2 sample

Fig. 10 The experimental and theoretical $-\Delta S_M(T)$ curves of La$_{0.57}$Nd$_{0.1}$Sr$_{0.33-x}$Ca$_x$MnO$_3$ (0.0 ≤ x ≤ 0.3) samples under 5 T magnetic fields

values of the samples are in agreement with each other at T_C and temperatures above T_C. This implies that the magnetoelastic coupling and electron interaction influence are an important factor for magnetocaloric properties [72]. However, below T_C, it is observed that there is a small-scale difference between the experimental and theoretical values. This may arise from the presence of AFM domains in the majority FM phase [73].

4 Conclusion

In this study, the structural, magnetic, and magnetocaloric properties of La$_{0.57}$Nd$_{0.1}$Sr$_{0.33-x}$Ca$_x$MnO$_3$ (0.0 ≤ x ≤ 0.3) samples were investigated. It was observed that there were small differences in the lattice parameter and unit cell volume of all samples crystallized in the rhombohedral symmetry. From the $M(T)$ measurements performed to determine the dependence of magnetization on temperature and T_C, it was detected that the samples showed a transition from the FM to PM phase with the increasing with temperature. The $-\Delta S_M^{max}$ values of the samples $-\Delta S_M$ were calculated as 2.53, 2.85, 3.17, and 5.85 J kg^{-1} K^{-1} under 2 T magnetic fields. For the same magnetic field change, the RCP values were also calculated. It is observed that the increasing of Ca content induces an increasing in the $-\Delta S_M^{max}$ and RCP values and a decrement in the T_C. The $-\Delta S_M^{max}$ and RCP value obtained for the LNSCM-2 sample

exhibiting a magnetic phase transition around room temperature is an acceptable size for MR applications in this temperature range. In addition, the $-\Delta S_M^{max}$ value of LNSCM-3 sample is larger than Gd for the same magnetic field change. This sample can be considered as a working material for the low-temperature magnetic refrigeration systems. The type of magnetic phase transition was determined using Banerjee's criterion, Franco's universal master curve, and Landau theory. All samples show second-order magnetic phase transition. All these experimental findings and theoretical calculations show that Ca ions are suitable doping agents for La$_{0.57}$Nd$_{0.1}$Sr$_{0.33-}$MnO$_3$ system. To increase both $-\Delta S_M$ and T_C (around T_C), different Ca contents (especially 0.15 ≤ x ≤ 0.3) will be prepared in next studies.

Data availability

All data included in this study are available upon request by contact with the author.

Code availability

Not applicable.

Declarations

Conflict of interest The author declares that she has no conflict of interest.

Ethical approval This article performed by the author does not contain any studies with human participants or animals. In this manuscript, I did not collect any samples of humans or animals. I summarized the research progress of structural, magnetic, and magnetocaloric properties of La$_{0.57}$Nd$_{0.1}$Sr$_{0.33-x}$Ca$_x$MnO$_3$ (0.0 ≤ x ≤ 0.3) samples.

References

1. A. Ressler, J. Macan, Perovskite oxides as active materials in novel alternatives to well-known technologies: a review. Ceram. Int. **48**, 27240–27261 (2022)

2. R. Khosla, N.D. Miranda, P.A. Trotter, A. Mazzone, R. Renaldi, C. McElroy, F. Cohen, A. Jani, R. Perera-Salazar, M. McCulloch, Cooling for sustainable development. Nature Sustainability **4**, 201–208 (2021)

3. K.A. Gschneidner, V.K. Pecharsky, Rare earths and magnetic refrigeration. J. Rare Earths **24**, 641–647 (2006)

4. B. Dorin, J. Avsec, A. Plesca, The efficiency of magnetic refrigeration and a comparison compressor refrigeration system. J. Energy Technol. **11**, 59–69 (2018)

5. A. Mleiki, R. M'nassri, W. Cheikhrouhou-Koubaa, A. Cheikhrouhou, E.K. Hlil, Structural characterization, magnetic, magnetocaloric properties and critical behavior in lacunar La0.5Eu0.2Ba0.2□0.1MnO3 nanoparticles. J. Alloys Compd. **727**, 1203–1212 (2017)

6. J. Romero Gómez, R. Ferreiro Garcia, A. De Miguel Catoira, M. Romero Gómez, Magnetocaloric effect: a review of the thermodynamic cycles in magnetic refrigeration. Renew. Sustain. Energy Rev. **17**, 74–82 (2013)

7. V.K. Pecharsky, K.A. Gschneidner, Magnetocaloric effect and magnetic refrigeration. J. Magn. Magn. Mater. **200**, 44–56 (1999)

8. M.H. Phan, S.C. Yu, Review of the magnetocaloric effect in manganite materials. J. Magn. Magn. Mater. **308**, 325–340 (2007)

9. V. Franco, J.S. Blázquez, J.J. Ipus, J.Y. Law, L.M. Moreno-Ramírez, A. Conde, Magnetocaloric effect: from materials research to refrigeration devices. Prog. Mater. Sci. **93**, 112–232 (2018)

10. B. Yu, Q. Gao, B. Zhang, X.Z. Meng, Z. Chen, Review on research of room temperature magnetic refrigeration. Int. J. Refrig **26**, 622–636 (2003)

11. K.A. Gschneidner, V.K. Pecharsky, Thirty years of near room temperature magnetic cooling: where we are today and future prospects. Int. J. Refrig **31**, 945–961 (2008)

12. B. Yu, M. Liu, P.W. Egolf, A. Kitanovski, A review of magnetic refrigerator and heat pump prototypes built before the year 2010. Int. J. Refrig **33**, 1029–1060 (2010)

13. L.T. Kuhn, N. Pryds, C.R.H. Bahl, A. Smith, Magnetic refrigeration at room temperature—from magnetocaloric materials to a prototype. J. Phys: Conf. Ser. **303**, 012082 (2011)

14. R.J.D. Tilley, *Perovskites: structure–property relationships* (John Wiley & Sons LTD, 2016)

15. C. Moure, O. Peña, Recent advances in perovskites: processing and properties. Prog. Solid State Chem. **43**, 123–148 (2015)

16. A. Barman, S. Kar-Narayan, D. Mukherjee, Caloric effects in perovskite oxides. Adv. Mater. Interfaces **6**, 1900291 (2019)

17. A.O. Ayaş, S. Kılıç Çetin, M. Akyol, G. Akça, A. Ekicibil, Effect of B site partial Ru substitution on structural magnetic and magnetocaloric properties in La0 7Pb0 3Mn1-xRuxO3 (x = 0 0, 0 1 and 0 2) perovskite system. J. Mol. Struct. **1200**, 127120 (2020)

18. S.K. Çetin, G. Akça, A. Ekicibil, Impact of small Er rare earth element substitution on magnetocaloric properties of $(La_{0.9-}Er_{0.1})_{0.67}Pb_{0.33}MnO_3$ perovskite. J. Mol. Struct. **1196**, 658–661 (2019)

19. G. Akça, S. Kılıç Çetin, A. Ekicibil, Structural, magnetic and magnetocaloric properties of (La1−xSmx)0.85K0.15MnO3 (x = 0.0, 0.1, 0.2 and 0.3) perovskite manganites. Ceram. Int. **43**, 15811–15820 (2017)

20. W. Zhong, C.T. Au, Y.W. Du, Review of magnetocaloric effect in perovskite-type oxides. Chin. Phys. B **22**(5), 057501 (2013)

21. K. Cherif, S. Zemni, Ja. Dhahri, Je. Dhahri, M. Oumezzine, M. Ghedira, H. Vincent, Magnetocaloric effect in the doped perovskite manganese oxide La0.7−xNdxSr0.3MnO3 (x=0.42, 0.56 and 0.7). J. Alloys Compd. **396**, 29–33 (2005)

22. Z.M. Wang, G. Ni, H. Sang, Y.W. Du, The effect of average A-site cation radius on T_C in perovskite manganites. J. Magn. Magn. Mater. **234**, 213–217 (2001)

23. V. Markovich, A. Wisniewski, H. Szymczak, Magnetic properties of perovskite manganites and their modifications. Handbook Magnet Mater. **22**, 1–201 (2014)

24. E. Tka, K. Cherif, J. Dhahri, E. Dhahri, H. Belmabrouk, E.K. Hlil, Effect of Al substitution on magnetocaloric effect in $La_{0.57}Nd_{0.1}Sr_{0.33}Mn_{1−x}Al_xO_3$ $(0.0 \leq x \leq 0.30)$ polycrystalline near room temperature. J. Alloy. Compd. **518**, 32–37 (2012)

25. R. Szymczak, M. Czepelak, R. Kolano, A. Kolano-Burian, B. Krzymanska, H. Szymczak, Magnetocaloric effect in $La_{1-x-}Ca_xMnO_3$ for x = 0.3, 0.35, and 0.4. J Mater Sci **43**, 1734–1739 (2008)

26. Z.B. Guo, Y.W. Du, J.S. Zhu, H. Huang, W.P. Ding, D. Feng, Large magnetic entropy change in perovskite-type manganese oxides. Phys. Rev. Lett. **78**(6), 1142–1145 (1997)

27. Y. Samancıoğlu, A. Coşkun, Magnetic properties of A- and B-site cation doped $La_{0.65}Ca_{0.35}MnO_3$ manganites. J. Alloy. Compd. **507**, 380–385 (2010)

28. E. Bouzaiene, A.H. Dhahri, J. Dhahri, E.K. Hlil, Structural, magnetic, magnetocaloric properties and critical behavior of La0.6Bi0.1Sr03-xCaxMn0.9Cu0.1O3 manganites (with x = 0.1 and 0.15). Inorg. Chem. Commun. **132**, 108824 (2021)

29. R.D. Shannon, Revised effective ionic radii and systematic studies of interatomic distances in halides and chaleogenides. Acta Cryst. **A32**, 751 (1976)

30. E.L. Hernández-González, S.A. Palomares-Sánchez, J.T. Elizalde Galindo, M. Mirabal-Garcia, Magnetocaloric effect near room temperature of La0.67Ca0.33−xSrxMnO3 (x = 0.06, 0.07, 0.08) Manganites. J Supercond Nov Magn **28**, 1635–1638 (2015)

31. K. Laajimi, M. Khlifi, E.K. Hlil, M.H. Gazzah, M.B. Ayed, H. Belmabrouk, J. Dhahri, Influence of Sr substitution on structural, magnetic and magnetocaloric properties in $La_{0.67-}Ca_{0.33-x}Sr_xMn_{0.98}Ni_{0.02}O_3$ manganites. J. Mater. Sci.: Mater. Electron. **31**, 15322–15335 (2020)

32. D.C. Linh, T.D. Thanh, L.H. Anh, V.D. Dao, H.G. Piao, S.C. Yu, Critical properties around the ferromagnetic-paramagnetic phase transition in $La_{0.7}Ca_{0.3-x}A_xMnO_3$ compounds (A = Sr, Ba and x = 0, 0.15, 0.3). J. Alloy. Compd. **725**, 484–495 (2017)

33. H.M. Rietveld, A profile refinement method for nuclear and magnetic structures. J. Appl. Cryst. **2**, 65–71 (1969)

34. J. Cibert, J.-F. Bobo, U. Lüders, Development of new materials for spintronics. C. R. Physique **6**, 977–996 (2005)

35. P. Chen, W. He, G. Xiao, J. Wen, T. Yang, X. Wu, T. Wang, Effect of A-site ionic disorder on the structure, magnetic, and magnetocaloric properties of La07-xNdxCa03-y(Ba, Sr)yMnO3. J. Appl. Phys. **127**, 055110 (2020)

36. A. Elghoul, A. Krichene, N. Chniba Boudjada, W. Boujelben, Rare earth effect on structural, magnetic and magnetocaloric properties of La0.75Ln0.05Sr02MnO3 manganites. Ceram. Int. **44**, 12723–12730 (2018)

37. A.E. Irmak, E. Taşarkuyu, A. Coşkun, M. Acet, Y. Samancıoğlu, S. Aktürk, Magnetic and electrical transport properties of $La_{0.65}Ca_{0.30}Pb_{0.05}Mn_{0.90}Cu_{0.10}O_3$ compounds: thermal hysteresis. Physica B **470–471**, 56–63 (2015)

38. A.D. Souza, P.D. Babu, S. Rayaprol, M.S. Murari, M. Daivajna, Study of combined effect of partial Bi doping and particle size reduction on magnetism of La0.7Sr0.3MnO3. J. Magnet. Magnet. Mater. **497**, 166020 (2020)

39. T. Raoufi, M.H. Ehsani, D.S. Khoshnoud, Magnetocaloric properties of $La_{0.6}Sr_{0.4}MnO_3$ prepared by solid state reaction method. J. Alloy. Compd. **689**, 865–873 (2016)

40. M.S. Islam, D.T. Hanh, F.A. Khan, M.A. Hakim, D.L. Minh, N.N. Hoang, N.H. Hai, N. Chau, Giant magneto-caloric effect around room temperature at moderate low field variation in $La_{0.7}(Ca_{1-x}Sr_x)_{0.3}MnO_3$ perovskites. Physica B **404**, 2495–2498 (2009)

41. T. Tang, R.S. Huang, S.Y. Zhang, Ultra-sharp metamagnetic transition in manganite Pr0.6Na0.4MnO3. J. Magn. Magn. Mater. **321**, 263–266 (2009)

42. M.A.A. Bally, M.A. Islam, M.Z. Ahasan, F.A. Khan, Effect of calcium doping on structural, magnetic and magneto-caloric properties of La0.55CaxSr0.45-xMnO3 manganites. J Magnet. Magnet. Mater. **557**, 169462 (2022)

43. M.H. Phan, V. Franco, N.S. Bingham, H. Srikanth, N.H. Hur, S.C. Yu, Tricritical point and critical exponents of La0.7Ca 0.3-xSrxMnO3 (x = 0, 0.05, 0.1, 0.2, 0.25) single crystals. J Alloys Compd **508**, 238–244 (2010)

44. J. Makni-Chakroun, W. Cheikhrouhou-Koubaa, M. Koubaa, A. Cheikhrouhou, Impact of a small amount of vacancy in both lanthanum and calcium on the physical properties of nanocrystalline $La_{0.7}Ca_{0.3}MnO_3$ manganite. J. Alloy. Compd. **650**, 421–429 (2015)

45. M. Shi, P. Bisht, A. Kumar, R.N. Mahato, Magnetic and magnetocaloric properties of the nanocrystalline $Pr_{0.7}Ba_{0.2-}Ca_{0.1}MnO_3$ sample. AIP Adv. **11**, 015239 (2021)

46. S.K. Çetin, M. Acet, M. Güneş, A. Ekicibil, M. Farle, Magnetocaloric effect in $(La_{1-x}Sm_x)_{0.67}Pb_{0.33}MnO_3$ ($0 \leq x \leq 0.3$) manganites near room temperature. J. Alloy. Compd. **650**, 285–294 (2015)

47. S. Mnefgui, A. Dhahri, N. Dhahri, E.K. Hlil, J. Dhahri, Effect of strontium deficiency on the critical behavior at paramagnetic to ferromagnetic phase transition in $La_{0.57}Nd_{0.1}Sr_{0.33}MnO_3$ manganite oxide. Solid State Sci. **21**, 19–25 (2013)

48. S. Gharbi, Y. Marouani, F. Issaoui, E. Dhahri, E.K. Hlil, R. Barille, B.F.O. Costa, Assessment of structural, optical, magnetic, magnetocaloric properties and critical phenomena of La0.57Nd0.1Sr0.18Ag0.15MnO3 system at room temperature. J Mater. Sci.: Mater. Electr. **31**, 11983–11996 (2020)

49. Z. Xie, Z. Zou, X. Jiang, W. Zhang, B. He, X. Han, Z. Mao, Structural, magnetic, and magnetocaloric properties of La0.7Sr0.2Nd0.1Mn1-xNixO3 (x= 0.05, 0.10, and 0.15): B-site doping. Phys. B Phys. Condensed Matter **639**, 413985 (2022)

50. M. El-Hagary, Y.A. Shoker, S. Mohammad, A.M. Moustafa, A. Abd El-Aal, H. Michor, M. Reissner, G. Hilscher, A.A. Ramadan, Structural and magnetic properties of polycrystalline La0.77Sr0.23Mn1-xCuxO3 ($0 \leq x \leq 0.5$) manganites. J. Alloys Compd. **468**, 47–53 (2009)

51. P.T. Phong, N.V. Dang, L.V. Bau, N.M. An, I.-J. Lee, Landau mean-field analysis and estimation of the spontaneous magnetization from magnetic entropy change in $La_{0.7}Sr_{0.3}MnO_3$ and $La_{0.7}Sr_{0.3}Mn_{0.95}Ti_{0.05}O_3$. J. Alloy. Compd. **698**, 451–459 (2017)

52. H. Guo, A. Gupta, M. Varela, S. Pennycook, J. Zhang, Local valence and magnetic characteristics of La_2NiMnO_6. Phys. Rev. B **79**, 172402 (2009)

53. V.S. Kolat, T. Izgi, O. Kaya, N. Bayri, H. Gencer, S. Atalay, Metamagnetic transition and magnetocaloric effect in charge-ordered $Pr_{0.68}Ca_{0.32-x}Sr_xMnO_3$ (x=0, 0.1, 0.18, 0.26 and

0.32) compounds. J. Magn. Magn. Mater. **322**, 427–433 (2010)

54. R. Mnassri, M.M. Nofal, P. De Rango, N. Chniba-Boudjada, Magnetic entropy table-like shape and enhancement of refrigerant capacity in La1.4Ca1.6Mn2O7-La1.3Eu0.1-Ca1.6Mn2O7 composite. RSC Adv. **9**, 14916–14927 (2019)

55. A.M. Tishin, Y.I. Spichkin, *The magnetocaloric effect and its applications* (IOP Publishing LTD, 2003)

56. M. Mansouri, H. Omrani, W. Cheikhrouhou-Koubaa, M. Koubaa, A. Madouri, A. Cheikhrouhou, Effect of vanadium doping on structural, magnetic and magnetocaloric properties of $La_{0.5}Ca_{0.5}MnO_3$. J. Magn. Magn. Mater. **401**, 593–599 (2016)

57. M.H. Phan, S.C. Yu, N.H. Hur, Excellent magnetocaloric properties of La0.7Ca0.3−xSrxMnO3 (0.05≤x≤0.25) single crystals. Appl. Phys. Lett. **86**, 072504 (2005)

58. A.O. Ayaş, M. Akyol, A. Ekicibil, Structural and magnetic properties with large reversible magnetocaloric effect in $(La_{1-x}Pr_x)_{0.85}Ag_{0.15}MnO_3$ (0.0 ≤ x ≤ 0.5) compounds. Phil. Mag. **96**(10), 922–937 (2016)

59. S. Mnefgui, A. Dhahri, N. Dhahri, E.K. Hlil, J. Dhahri, The effect deficient of strontium on structural, magnetic and magnetocaloric properties of $La_{0.57}Nd_{0.1}Sr_{0.33-x}MnO_3$ (x=0.1 and 0.15) manganite. J. Magn. Magn. Mater. **340**, 91–96 (2013)

60. E. Tka, K. Cherif, J. Dhahri, Evolution of structural, magnetic and magnetocaloric properties in Sn-doped manganites $La_{0.57}Nd_{0.1}Sr_{0.33}Mn_{1-x}Sn_x$ O3 (x = 0.05-0.3). Appl. Phys. A Mater. Sci. Process. **116**(3), 1181–1191 (2014)

61. C.G. Ünlü, Y.E. Tanış, M.B. Kaynar, T. Şimşek, Ş Özcan, Magnetocaloric effect in $La_{0.7}Nd_xBa_{(0.3-x)}MnO_3$ (x = 0, 0.05, 0.1) perovskite manganites. J. Alloy. Compd. **704**, 58–63 (2017)

62. J. Dhahri, A. Dhahri, M. Oummezzine, E.K. Hlil, Effect of substitution of Fe for Mn on the structural, magnetic properties and magnetocaloric effect of $LaNdSrCaMnO_3$. J. Magn. Magn. Mater. **378**, 353–357 (2015)

63. A.M. Tishin, V.K. Pecharsky, K.A. Gschneidner, Magnetic phase transitions and the magnetothermal properties of gadolinium. Phys. Rev. B **57**(6), 3478–3490 (1998)

64. J.Y. Law, V. Franco, L.M. Moreno-Ramirez, A. Conde, D.Y. Karpenkov, I. Radulov, K.P. Skokov, O. Gutfleisch, A quantitative criterion for determining the order of magnetic phase transitions using the magnetocaloric effect. Nat. Commun. **9**, 2680 (2018)

65. B.K. Banerjee, On a generalised approach to first and second order magnetic transitions. Phys. Lett. **12**, 16–17 (1964)

66. V. Franco, A. Conde, J.M. Romero-Enrique, J.S. Blázquez, A universal curve for the magnetocaloric effect: an analysis based on scaling relations. J. Phys. Condens. Matter **20**, 285207 (2008)

67. V. Franco, A. Conde, V.K. Pecharsky, K.A. Gschneidner, Does a universal curve exist? EPL **79**, 47009 (2007)

68. V.S. Amaral, J.S. Amaral, Magnetoelastic coupling influence on the magnetocaloric effect in ferromagnetic materials. J. Magn. Magn. Mater. **272–276**, 2104–2105 (2004)

69. J.S. Amaral, M.S. Reis, V.S. Amaral, T.M. Mendonça, J.P. Araújo, M.A. Sá, P.B. Tavares, J.M. Vieira, Magnetocaloric effect in Er- and Eu-substituted ferromagnetic La-Sr manganites. J. Magnet. Magnet. Mater **290–291**, 686–689 (2005)

70. A. Davarpanah, J.H. Belo, V.S. Amaral, J.S. Amaral, On the optimization of magneto-volume coupling for practical applied field magnetic refrigeration. Phys. Status Solidi B **256**, 1800419 (2018)

71. A. Fujita, K. Fukamichi, Large magnetocaloric effects and Landau coefficients of itinerant electron metamagnetic $La(Fe_xSi_{1-x})_{13}$ compounds. IEEE Trans. Magnet. **41**(10), 3490–3492 (2005)

72. H. Ben Khlifa, Y. Regaieg, W. Cheikhrouhou-Koubaa, M. Koubaa, A. Cheikhrouhou, Structural, magnetic and magnetocaloric properties of K-doped Pr08Na02−xKxMnO3 manganites. J. Alloys Compd. **650**, 676–683 (2015)

73. A. Elghoul, A. Krichene, W. Boujelben, Landau theory and critical behavior near the ferromagnetic-paramagnetic transition temperature in $Pr_{0.63}A_{0.07}Sr_{0.3}MnO_3$ (A=Pr, Sm and Bi) manganites. J. Phys. Chem. Solids **108**, 52–60 (2017)